SLAC – PUB – 4564
March 1988
(T/E)

ELECTRON-POSITRON PHYSICS AT 1 TeV*

Gary J. Feldman
Stanford Linear Accelerator Center
Stanford University, Stanford, California 94305

ABSTRACT

We discuss the motivation for TeV e^+e^- linear colliders, some aspects of their design, and the experimental consequences that follow from the design. After a brief discussion of the general physics environment, we consider the discovery potential of these colliders by examining three sample processes: the detection of new heavy leptons, standard Higgs bosons, and charged Higgs bosons.

1. INTRODUCTION

About a year ago, Burton Richter established two committees at SLAC to begin work on a proposal for a high-energy linear e^+e^- collider. One group, the Collider Accelerator Coordinating Committee, was charged with coordinating the study of accelerator issues and with coordinating the necessary accelerator research and development work. The other committee, the Collider Physics Coordinating Committee, was charged with studying the physics potential of such a collider and with making recommendations concerning the parameters that it should have. The members of these committees are listed in Table 1. The Accelerator Committee stayed small, acting as a true coordinating committee. The

* Work supported by the Department of Energy contract DE–AC03–76SF00515.

Presented at the 8th International Conference
on High Energy Physics at Vanderbilt
Collider Physics: Present Status and Future Prospects,
Nashville, Tennessee, October 8–10, 1987

Table 1: Collider Committee Memberships

Collider Physics Coordinating Committee	Collider Accelerator Coordinating Committee
Changrim Ahn	Tom Himel (Physics liaison)
Charles Baltay	Bob Palmer
Tim Barklow	Ewan Paterson (chairman)
Pat Burchat	John Rees
David Burke	Ron Ruth
Adrian Cooper	Rae Stiening
Claudio Dib	Perry Wilson
Gary Feldman	
Jack Gunion	
Howard Haber	
Tom Himel	
Sachio Komamiya	
Bryan Lynn	
Michael Peskin (chairman)	
Alfred Petersen	
John Rees (Accelerator liaison)	
Rick Van Kooten	

Physics Committee, on the other hand, grew throughout the year by exercising the option given to it by its charter to co-opt additional members.

This talk will report on some of the work that has been done by these two committees.[1)] However, these reports should be considered unofficial and preliminary since neither committee has yet issued a report. All the conclusions that I draw in this talk are my own and may differ from the conclusions the committees subsequently draw in their reports. Similarly, I have made numerous calculations in this talk; any errors I have made are entirely my own.

The next section will outline the motivation for e^+e^- linear colliders in the TeV region. In Section 3, I will briefly review the present thinking on high-

energy e^+e^- linear colliders, stressing those points that have consequences for detector design and physics analyses. Section 4 will discuss the general physics environment. Finally, sections 5 through 7 will discuss three examples of the discovery potential of these colliders — heavy leptons, standard Higgs bosons, and charged Higgs bosons.

2. PHYSICS MOTIVATION

The major question facing particle physics in the next decade or two is the question of mass. In the standard model W and fermion masses are given by

$$m_W = \frac{g}{2} < \phi > \tag{1}$$

and

$$m_f = \frac{\lambda_f}{2} < \phi > \tag{2}$$

where g is the weak coupling parameter, λ is an arbitrary parameter for each fermion, and $< \phi >$ is the Higgs field vacuum expectation value. The value of $< \phi >$ results from the physics of a new sector.

The totality of our knowledge about this sector is

$$< \phi >= 246 \text{ GeV} \tag{3}$$

and

$$\rho \cong 1. \tag{4}$$

The former relation sets the mass scale for the Higgs sector and the latter relation tells us that this sector has a global SU(2) symmetry.

There are many ways that Nature could have chosen to implement the Higgs sector:

1. The minimal scheme has one doublet of Higgs fields and leads to one physical neutral Higgs boson. This is not very satisfying, because the origin of the Higgs self-coupling and the fermion mass terms is not explained.

2. The simplest non-minimal scheme has two doublets of Higgs fields leading to five physical Higgs bosons, three neutral and one pair of charged bosons. This scheme has the same problems as the first, but with more parameters.

3. Finally the symmetry breaking can be caused by dynamics. Two examples of this are supersymmetry, in which the Higgs fields are elementary and arise out of their coupling to supermatter, and technicolor, in which the Higgs fields are composite.

Regardless of the nature of the Higgs fields, the important point is that there must be a new sector below or around 1 TeV. In addition to neutral Higgs bosons, this sector could generate

1. new quarks and leptons
2. new gauge bosons
3. supersymmetric partners
4. exotic fermions, and
5. technipions, or charged Higgs bosons,

all in the sub-TeV mass region.

Electron-positron colliders are complementary to hadron colliders in uncovering and studying this physics. Hadrons colliders may well make the initial discoveries of new physics, but e^+e^- colliders will be very useful in making detailed investigations. There are three main reasons for this:

1. Strong peripheral processes, which cause large backgrounds in hadron colliders, are absent in e^+e^- colliders.

2. The partons in e^+e^- collisions are the electron and positron themselves. Since these are quite hard, familiar and new particles are produced at approximately the same rate.

3. Longitudinal polarization of the electron beam is feasible and useful for studying couplings of new particles.

The major physics drawback of e^+e^- collisions is the rather small cross sections. The basic unit of cross section is the cross section for the electromagnetic production of an muon pair:

$$1R = \frac{4\pi\alpha^2}{3s} = \frac{87 \text{ fm}}{[E(\text{TeV})]^2}. \tag{5}$$

At 1 TeV center-of-mass energy, 1000 units of R corresponds to 10^7 seconds of $10^{33}\text{cm}^{-2}\text{sec}^{-1}$of luminosity. To obtain average luminosities of $10^{33}\text{cm}^{-2}\text{sec}^{-1}$, it may be necessary to design colliders for a peak luminosity of $10^{34}\text{cm}^{-2}\text{sec}^{-1}$.

3. LINEAR COLLIDER PARAMETERS AND EXPERIMENTAL CONSEQUENCES

3.1. Why Linear Colliders?

The first question we have to ask is why we want to consider linear colliders as opposed to storage rings for high-energy e^+e^- collisions. Richter studied the scaling laws for storage rings in 1976.[2] There are two factors in the cost of a high-energy storage ring. Most of the costs scale as the size of the ring — tunnels, magnets, vacuum systems, etc. The one cost that does not scale with the size of the ring is the rf system, which is required to make up the energy lost to synchrotron radiation. The voltage required to restore the lost energy is proportional to the fourth power of the energy and inversely proportional to the radius of curvature. Thus, simplifying Richter's argument considerably, we can write

$$C = \alpha R + \beta \frac{E^4}{R}, \tag{6}$$

where C is the cost, R is the radius, E is the energy, and α and β are constants. Optimizing the cost by setting the derivative of Eq. (6) with respect to R to zero yields the result that both the cost and size of a storage ring scale with E^2.

We can thus estimate the cost of a 1 TeV storage ring by assuming that LEP II is an optimized 200 GeV storage ring and using this scaling law. The

result is that such a ring would be 675 km in circumference and cost 17.5 billion dollars. Even by our new sense of reasonableness set by the SSC scale, this seems unreasonable and suggests that we should pursue an alternate technology. Both the cost and size of a linear collider, of course, scale with energy, making it appear to be a more promising approach.

3.2. Linear Collider Parameters

Figure 1 shows a generic linear collider. It has three main accelerators: an electron linac to produce positrons, and positron and electron linacs to accelerate the beams to high energy. It also has two damping rings to reduce the emittance of the beams, although in some designs the electron damping ring may not be necessary.

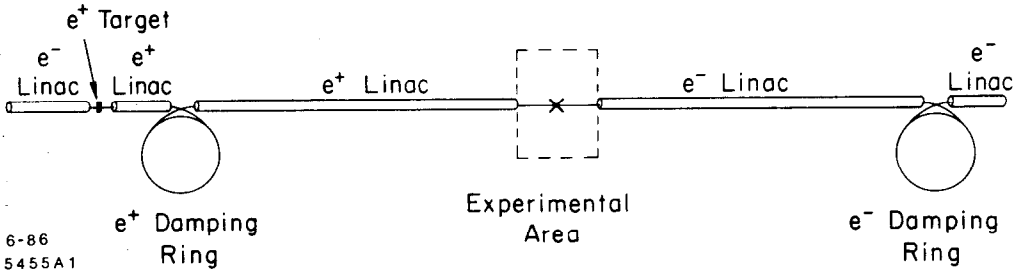

Fig. 1. Schematic of a generic linear collider.

Figure 2 shows the only present example of a linear collider, the SLC. Please note that this design is topologically equivalent to the generic linear collider with the present SLAC linac serving as all three required linacs. A positron return line and two arcs have been added to transport the particles to the required locations; in principle, these transport lines do not affect the basic functioning of the collider.

I will not say anything about the SLC in this talk except to use it as a comparison to the designs for very high-energy colliders. There are two design

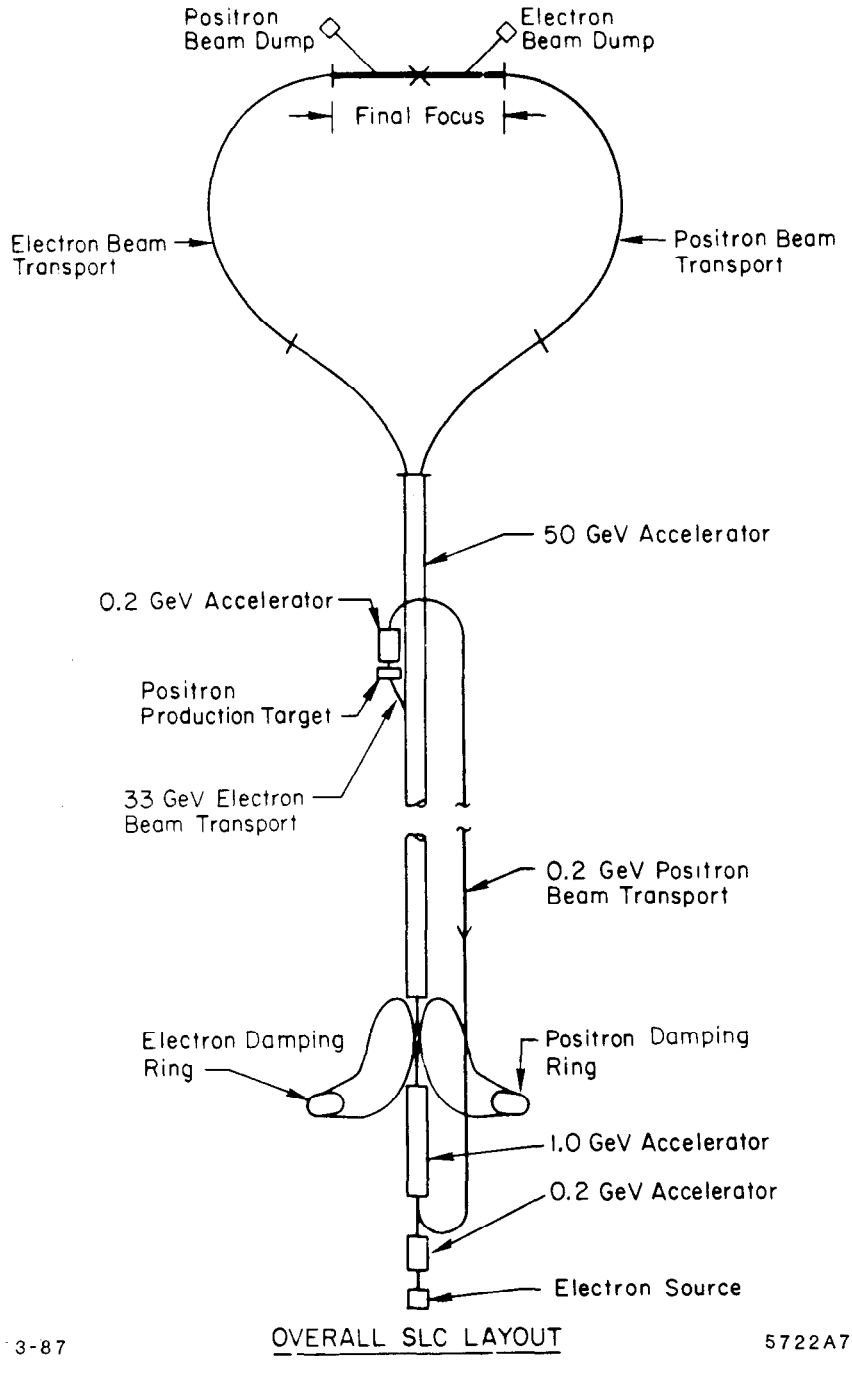

Fig. 2. Schematic of the SLC.

exercises we can look at: the Cern Linear Collider (CLIC), a 2 TeV collider being designed at CERN,[3] and the TeV Linear Collider (TLC).* Table 2 lists some parameters of the SLC† and these two designs. All three use a conventional travelling wave rf structure for the main accelerator, but differ on the source of rf power. SLC uses conventional klystrons; the CLIC design uses a superconducting drive linac in which a low-energy, high-current electron beam transmits energy to the main linac; and the TLC design envisions using a relativistic klystron in which the low-energy beam is driven by magnetic induction.

The accelerator gradients are considerably higher in the high-energy colliders in order to keep the length reasonable. The TLC design at 196 MV/m is considerably higher than the 80 MV/m envisioned in the CLIC design. Part of the reason for this is to have a design for a 1 TeV collider that would fit on Stanford University land.

The repetition rate is mainly determined by power, or equivalently, money. For a given design, one can pulse more frequently at the cost of increased power and, possibly, additional components.

Multibunch operation is certainly attractive in principle as a way of increasing the luminosity, but there are technical problems to be solved with wake-field control and the requirement that each pulse have the same accelerating field. The latter is required by the necessarily small momentum acceptance of the final focus.

The number of electrons or positrons per bunch is primarily limited by wake field effects. Transverse wake fields are caused by a beam traveling off center through the accelerating structure. The tail of the beam sees the fields excited by the head, leading to an apparent emittance growth.

To keep the design luminosity as high as possible one likes to make the transverse beam sizes, σ_x and σ_y, as small as possible. The technical challenge is to

---

* The SLAC collider design does not have an official name, but we have to call it something. Mike Peskin gets credit for coming up with TLC.

† In this talk the design parameters of the SLC will be used although some of the design parameters such as the 180 Hz repetition rate may never be achieved due to fiscal constraints.

Table 2: Summary of Collider Parameters

	SLC	CLIC	TLC
Location	SLAC	CERN (?)	SLAC (?)
Status	Commissioning	Early design studies	
$E_{c.m.}$ (TeV)	0.1	2	1
Power source	Klystron	Superconduct. drive linac	Relativistic klystron
Accelerator type	Conventional travelling wave rf structure		
Accelerator gradient (MV/m)	17	80	196
Accelerator length (km)	3	2×12.5	2×2.5
Rf wavelength (cm)	10	1	2.5
Repetition rate (Hz)	180	5800	90
Particles per bunch	7×10^{10}	5.4×10^{9}	1.8×10^{10}
Beam power (MW)	2×0.10	2×5	2×0.13
Horiz. emittance ϵ_x (rad m)	4.2×10^{-5}	2.8×10^{-6}	5×10^{-6}
Vert. emittance ϵ_y (rad m)	4.2×10^{-5}	2.8×10^{-6}	5×10^{-8}
β_x^* (mm)	5	3	15
β_y^* (mm)	5	3	0.05
Bunch width σ_x^* (μm)	1.7	0.065	0.270
Bunch height σ_y^* (μm)	1.7	0.065	0.0016
Bunch length σ_z (mm)	1	0.5	0.04
Disruption	0.76	0.91	10
Pinch enhancement	2.2	3.5	2.3
Quantum radiation param. Υ	6×10^{-3}	0.28	1.6
Beamstrahlung δ	4×10^{-3}	0.19	0.27
Max. disruption angle (mrad)	1.2	0.12	0.38
Luminosity ($cm^{-2}sec^{-1}$)	6×10^{30}	1.1×10^{33}	1.2×10^{33}

do so. The beam size at the interaction point is given by

$$\sigma_{x,y} = \left(\frac{\epsilon_n \beta^\star}{\gamma}\right)^{\frac{1}{2}}_{x,y}, \tag{7}$$

where ϵ_n, is the normalized emittance, *i.e.*, $\epsilon\gamma$, the quantity that is conserved during acceleration, and $\beta^\star$ is the β function, or focal length, at the interaction point.

Both of the high-energy colliders have emittances about an order of magnitude smaller than the SLC, except that the vertical emittance of the TLC is two orders of magnitude smaller still. The vertical emittance of a storage ring is limited mainly by the coupling into the vertical from the horizontal. The technical question is whether this factor of 100 reduction can be both produced and maintained through the acceleration and focusing processes.

Why is the TLC proposing flat beams rather than the standard round beams? (Note that the standard is set by a single example.) There are a number of reasons:

1. The emittance of damping rings is much smaller in the vertical than in the horizontal.

2. Magnetic quadrupoles focus in one plane while defocusing in the orthogonal plane. Thus an asymmetric focus is natural.

3. A finite crossing angle is needed for high luminosity. This is because in a high-luminosity system the beam disruption will cause the outgoing beam to be larger than the aperture of the final quadrupole. For example, at the TLC the maximum disruption angle is approximately given by

$$\theta_{d_{max}} \approx \frac{2Nr_e}{\gamma\sigma_x} \approx 0.4 \text{ mrad}. \tag{8}$$

This translates into a circle of 220 μm at the face of the first quadrupole, which is located longitudinally 55 cm from the interaction point; however,

the inner diameter of these quadrupoles is only 180 μm. A finite crossing angle solves this problem, but creates another one. To avoid losing luminosity,

$$\sigma_x \geq \theta_c \sigma_z, \tag{9}$$

where θ_c is the crossing angle. This condition can be best met by flat beams, as illustrated in Fig. 3. The TLC crossing angle is 6 mrad, which, when combined with the designed beam sizes, meets the above requirement.

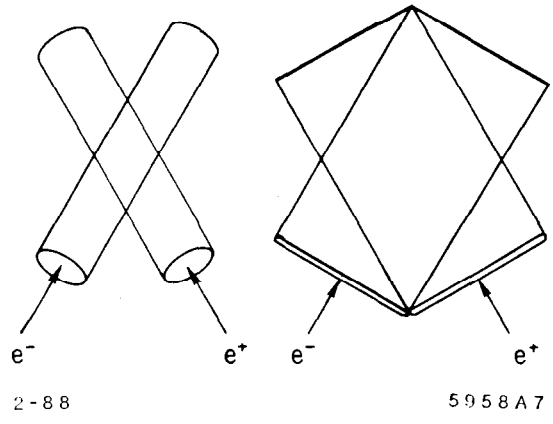

Fig. 3. The effective overlap of different shaped crossing beams.

The fourth reason for having flat beams is the effect on beamstrahlung, which we treat here in its own right. Figure 4 shows how particles from one beam see the other beam as a focusing lens. This focusing field produces synchrotron radiation known as "beamstrahlung."* The average energy loss by beamstrahlung, δ, is given by[4]

$$\delta = \frac{0.22 r_e^3 N^2 \gamma}{\sigma_z \sigma_y'} \left[\frac{4}{\left(1 + \frac{\sigma_x'}{\sigma_y'}\right)^2} \right] \left(\frac{1}{1 + 1.33 \Upsilon^{\frac{2}{3}}} \right)^2, \tag{10}$$

where

$$\Upsilon = \frac{0.43 r_e^2 N \gamma}{\alpha \sigma_z \sigma_y'} \left(\frac{2}{1 + \frac{\sigma_x'}{\sigma_y'}} \right). \tag{11}$$

* J. R. Rees claims responsibility for this unfortunate coinage.

The primes on the σ's in the above equations indicate that the pinched values are to be used.

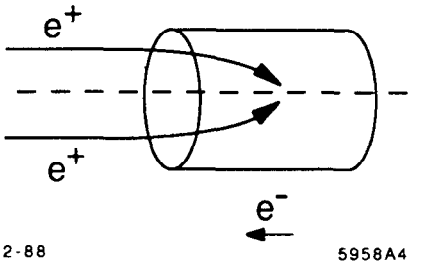

Fig. 4. Focusing of an electron by the charge of the opposite beam.

It is clear from the above that flat beams give lower average energy loss. This is because for the areas involved, on the average, the charge is further away. Another way of seeing the same thing is to note that the electric field above and below a flat beam does not change as the thickness of the beam shrinks.

Υ is a measure of the quantum versus classical nature of the beamstrahlung. The last term in Eq. (11) gives the suppression due to quantum effects. This is a factor of eight in the TLC design.

The solid line in Fig. 5 shows the spectrum of center-of-mass energy after beamstrahlung versus the integrated luminosity for parameters similar to those of the TLC. The average energy loss δ is 0.26. Note that 32% of the spectrum is in the last bin, *i.e.*, there is no beamstrahlung. The dashed line in Fig. 5 shows the effect of multiplying this spectrum by E^{-2} to simulate the effect of the E^{-2} dependence of the cross section for annihilation processes. The resulting rate of production versus energy is approximately flat except for the rise at the maximum energy.

An immediate consequence of the spectrum of Fig. 5 is shown in Fig. 6. This figure, prepared by Tom Himel, shows the event rate as a function of energy if a Z′ resonance exists at a mass of 400 GeV/c^2. The couplings of a Z′ to e^+e^- are

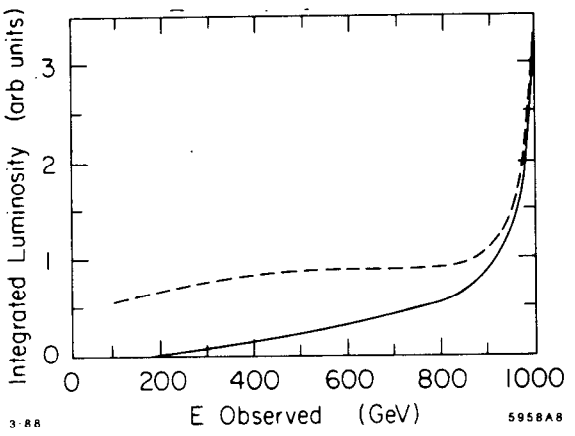

Fig. 5. A typical beamstrahlung spectrum for the TLC design. $\delta = 0.26$. The dashed curve represents the spectrum multiplied by E^{-2} to approximate the cross section for annihilation processes.

model dependent,[5] but an enhancement of several hundred over the continuum, as shown in Fig. 6, is typical. It is clear from this graph that beamstrahlung makes high-energy linear colliders self-scanning.

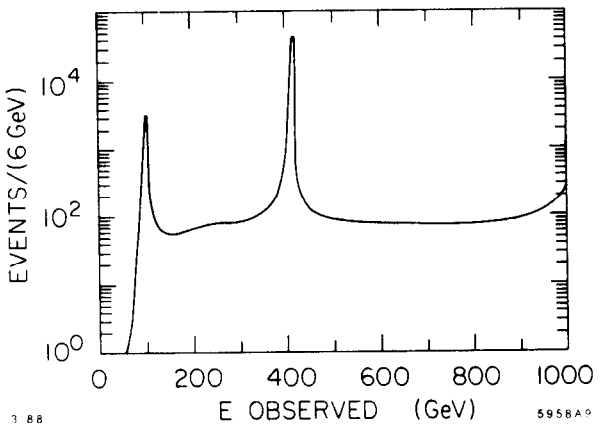

Fig. 6. The event rate for $e^+e^- \rightarrow$ hadrons in the TLC if a Z′ resonance with mass of 400 GeV/c^2 exists.

I will not discuss Z′ resonances further in this talk because they are clearly very easy to find, and the physical measurements that one would make are quite

similar to those that will be made on the Z by the SLC and LEP. If we were to discover a Z′ resonance at the Tevatron or the SSC, then we could consider building a dedicated e^+e^- linear collider to study it. This collider could have lower luminosity than the luminosities we are considering here and would, consequently, be much simpler to build and operate.

3.3. Experimental Consequences

There are two main experimental consequences of the TLC design that we have had to incorporate into our simulations of TLC physics. First, we have used beamstrahlung spectra with $0.22 < \delta < 0.26$. We have used two approaches to deal with beamstrahlung. In most analyses, we have given up on the constraints on $E_{c.m.}$ and $(p_z)_{c.m.}$ and have just used the conservation of transverse momenta, as is done in hadron colliders. In one analysis I will discuss (charged Higgs bosons), all of the constraints were retained in a mild way by only using events in which the visible energy was approximately equal to the total energy.

The second consequence has to do with the forward direction. Since the final quadrupoles in the TLC design are only 55 cm from the interaction point, since these quadrupoles have to be supported on actively vibration-damped supports, and since the design has crossing beams, we have assumed that no particles are detected within 10° of the incident beams. It is probable that we will be able to do some particle detection in this region, but we wanted to be conservative and see whether this condition prevented us from doing any physics.

4. GENERAL PHYSICS ENVIRONMENT

4.1. Detector Requirements

Much of the physics of the TLC will require the detection of W's and Z's. These particles will be the "pions" of lower-energy colliders. We will want to be able to detect them in their hadronic decays for two reasons:

1. The rate is higher. Seventy-five per cent of W decays and 85% of visible Z decays go into hadrons.

2. The W leptonic decay, $W \rightarrow \ell\nu$, has undetected neutrino energy. Thus, we lose a usually required constraint and we cannot reconstruct masses.

The key to reconstructing W and Z masses is a well-segmented hadronic calorimeter. A study of how much segmentation is needed indicated that a calorimeter with 4° by 4° cells gives adequate segmentation.[6] This is approximately the segmentation of the SLD detector.

An energy resolution of $0.5/\sqrt{E}$ is quite adequate. However, an important point about calorimeters at high energy should be noted. In general, one can approximate the energy of a calorimeter by

$$\frac{\delta E}{E} = \frac{a}{\sqrt{E}} + b. \tag{12}$$

If $a = 0.50$, then at an energy of 1 TeV, b must be less than 0.015 so as not to dominate the $a/\sqrt{E}$ term. Wigmans has shown than an e/π response that differs from unity will set a lower limit on b.[7] For example, the lead-liquid argon SLD calorimeters have an e/π response of 1.24, which implies that $b \geq 0.045$. To get $b < 0.015$, the e/π response must lie between 0.9 and 1.1. It is now known how to build a variety of calorimeters that meet this condition.[7]

4.2. Charged Particle Tracking

Another requirement we will have is to measure 500 GeV leptons relatively well. A charged particle momentum resolution of $\Delta p/p = 3 \times 10^{-4}$, ($p$ in GeV/c) yields an rms resolution of 15% at 500 GeV/c, which is quite adequate. Scaling from the Mark II design and using a tight vertex constraint, one can achieve this with a drift chamber with the following parameters:

1. a radius of 1.8 m,
2. a B field of 1.0 T, and
3. 72 layers with 200 μm resolution on each layer.

These parameters are relatively easy to achieve.

Table 3: First-order and Actual Cross Sections for the Major Annihilation Processes

Process	R_0	R	Events/2 fb^{-1}
$e^+e^- \rightarrow q\bar{q}$	8.9	46.2	8000
$e^+e^- \rightarrow W^+W^-$	26.6	41.1	7100
$e^+e^- \rightarrow ZZ$	1.5	2.4	400

4.3. Basic Processes

To understand the general physics environment we will face at the TLC, we will look at the two major annihilation processes:

$$e^+e^- \rightarrow q\bar{q} \tag{13}$$

and

$$e^+e^- \rightarrow W^+W^- \tag{14}.$$

Pat Burchat has prepared some plots of these processes at a center-of-mass energy of 1 TeV with detector smearing, beamstrahlung, and bremsstrahlung for 2 fm^{-1} of data (Figs. 7-10). For orientation, this amount of data would be accumulated in 2 months of running at an average luminosity of 4×10^{32} $cm^{-2}sec^{-1}$.

Table 3 gives the first-order cross sections and the actual observed cross sections for these processes and the smaller Z pair production process. As usual, the cross sections are given in terms of R, the ratio between the cross section and the first-order electromagnetic μ-pair production cross section. There is a large difference between the first-order cross section (R_0) and the observed cross section (R). This is partially due to the effect of beamstrahlung, which effectively reduces the center-of-mass energy and thus increases the cross section. In the case of quark-pair production, the bulk of the observed cross section is due simply to the production of the Z and a hard photon. We will see that it is easy to discriminate this relatively uninteresting process.

Figures 7, 8, and 10 show quantities for reactions (13) and (14), the former on the top half of the figure and the latter on the bottom half. Figure 7 shows the visible energy, the invariant mass of the visible particles, and the cosine of the trust axis. The quark-pair (*i.e.*, hadron) production is dominated by the beforementioned process of radiating to the Z. This process gives a strong forward peaking and invariant masses of at most the Z mass. The W pair production is also strongly forward peaked because it is dominated by the diagram in which a neutrino is exchanged. Most of the new physics that we will be searching for will occur in the central region. To see this region more clearly, in Figures 8 through 10 we apply two cuts, as indicated on Figure 7:

$$\cos\theta_{thrust} \leq 0.8, \tag{15}$$

and

$$m \geq 0.3E_{c.m.}, \tag{16}$$

where m is the invariant mass of all of the visible particles.

Figures 8(a) and (b) show the charged multiplicity. For quark-pair production, the average charged multiplicity is 41, about twice as large as it is on the Z. For W-pair production, the average charged multiplicity is 29, but this is made up of three distinct cases: Six per cent of the events have both W's decay leptonicly and have low multiplicity, typically 2; about 40% of the events have one W decay leptonicly and the other hadronicly, giving a charged multiplicity of slightly more than 20; and the remainder of the events have both W's decay hadronicly, yielding a charged multiplicity of about 40, similar to the quark-pair case.

Figures 8(c) and (d) show the invariant mass of each hemisphere defined by the plane normal to the thrust axis. The bump at the Z mass in quark-pair production is due to the fundamental process $e^+e^- \rightarrow Z\gamma$ at large angles, so that it satisfies conditions (15) and (16). This process can be easily separated from normal quark-pair production, as will be seen in Figure 9. The quark-pair production jet masses peak around 40 GeV/c^2 with a long tail due to gluon

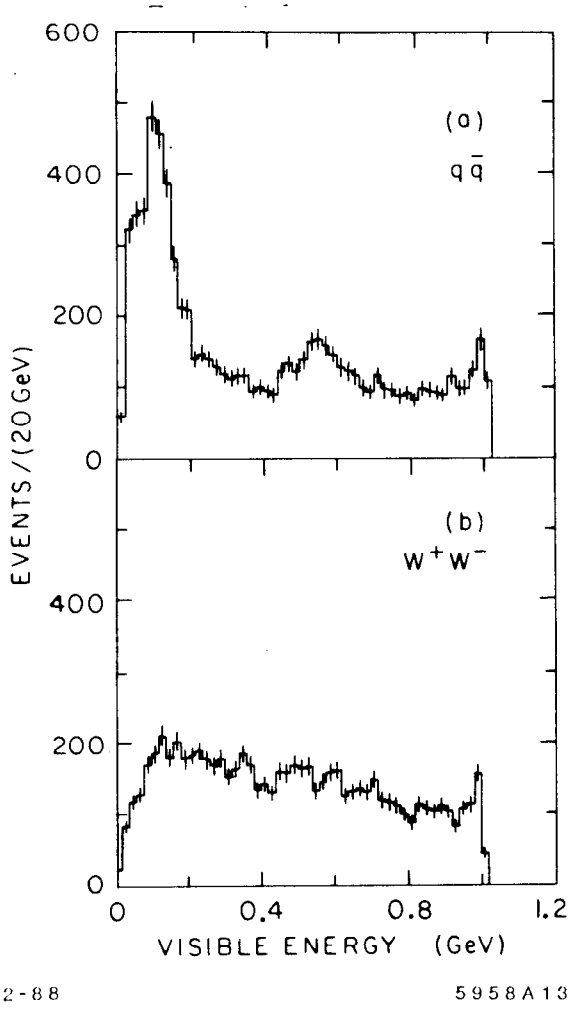

Fig. 7(a-b). The visible energy for (a) quark-pair production and (b) W-pair production.

production. In contrast, the invariant masses in each hemisphere from W-pair production peak sharply at the W mass with small tails due to confusion from backward-going particles.

Figure 9 shows scatter plots of the masses in each hemisphere for each of the three processes listed in Table 3. It is clear that W-pair events can be separated from quark-pair production rather cleanly by this technique alone. The Z-pair production appears to be lost in the tails of the more copious processes, but we will see shortly that there is even a possibility of separating it in its hadronic

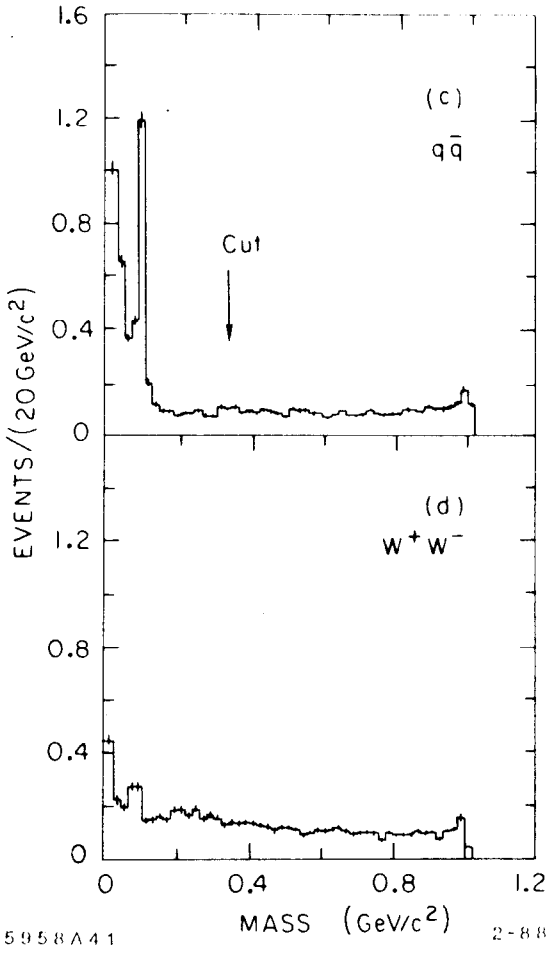

Fig. 7(c-d). The visible invariant mass for (c) quark-pair production and (d) W-pair production.

decay modes.

Figure 10 shows various measures of transverse momentum. In Figs. 10(a) and (b) the sum of the transverse momentum of visible particles is plotted. There is a substantial tail beyond 40 GeV/c from neutrino production. Figures 10(c) and (d) differ in plotting the momentum transverse to both the incident beams and the thrust axis. Here there is no tail beyond 40 Gev/c, because neutrinos are emitted preferentially in the thrust direction. A somewhat equivalent variable is plotted in Figs. 10(e) and (f), the acoplanarity angle of the sum of the momentum in each

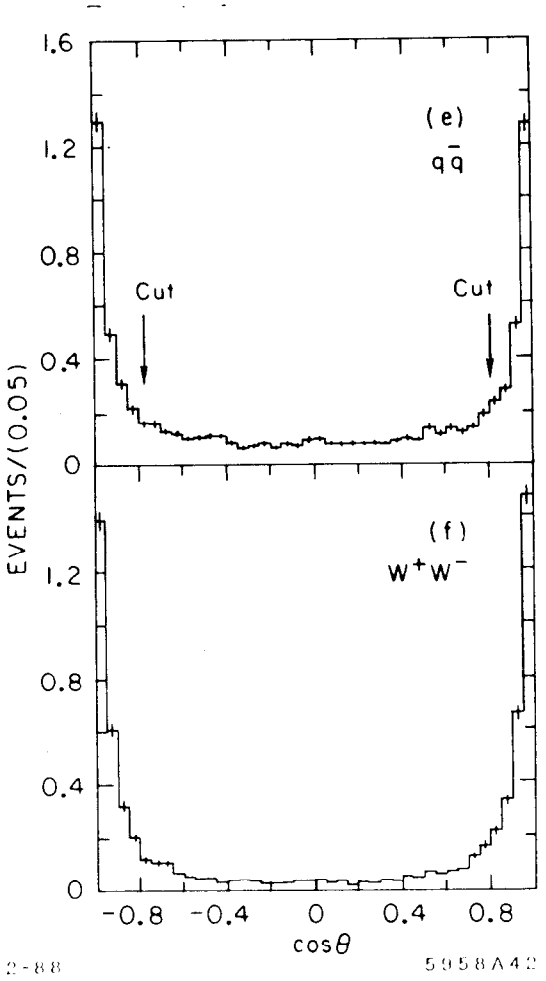

Fig. 7(e-f). The cosine of the thrust axis for (e) quark-pair production and (f) W-pair production.

hemisphere. There are relatively few events beyond 10° for quark-pair production and 20° for W-pair production. The moral of Fig. 10 is that when searching for new processes for which non-zero transverse momentum is a signature, it is generally better to use either the transverse momentum normal to the thrust axis or the acoplanarity angle as a discriminant rather than just the transverse momentum.

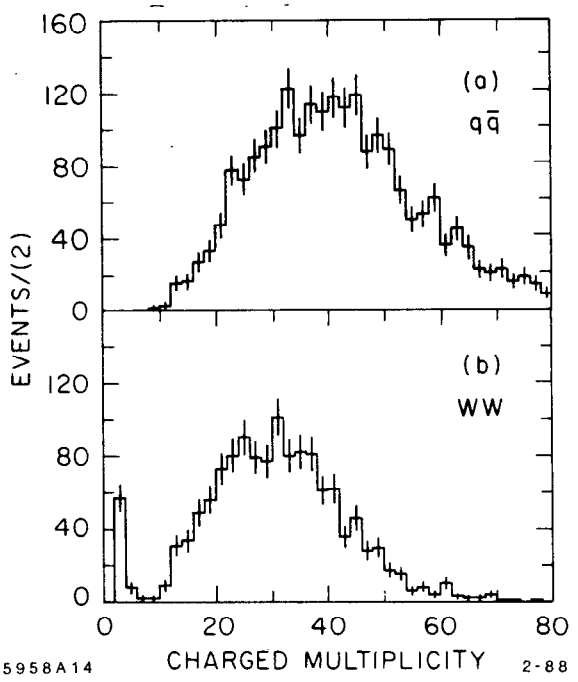

Fig. 8(a-b). The charged multiplicity for (a) quark-pair production and (b) W-pair production.

4.4. Two-Photon Processes

Figure 11 shows diagrams for two-photon or "$\gamma\gamma$-fusion" production of quark and W pairs. The cross section for hadron production is enormous, but the mass of the system is small. This will not be any more of a problem at the TLC than it has ever been in e^+e^- annihilations.

The production of W pairs by $\gamma\gamma$ fusion received a great deal of attention at the La Thuile Workshop,[8] but it will be unimportant for our purposes because the electrons have no transverse momenta and go forward. Thus this process looks exactly like $e^+e^- \rightarrow W^+W^-$ in the presence of beamstrahlung, except that it is softer and has a smaller cross section. Figure 12 shows the invariant mass spectrum of W pairs from $\gamma\gamma$ fusion. It is to be compared with Figure 7(e). Note that the W^+W^- invariant mass spectrum is much flatter, varying from 200 to 100 events per 20 GeV/c^2 bin from threshold to 1 TeV/c^2. Table 4 gives a comparison

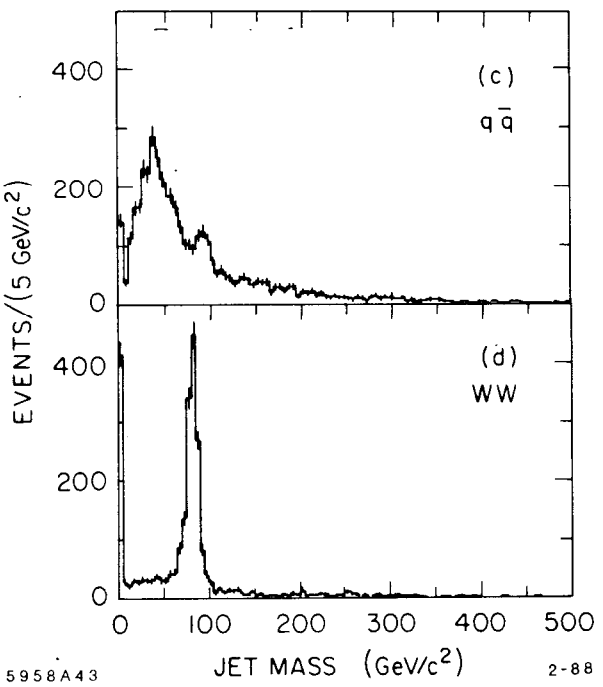

Fig. 8(c-d). The jet mass in each hemisphere defined by the normal to the thrust axis for (c) quark-pair production and (d) W-pair production.

of the cross sections.

Based on these results, we can safely ignore the $\gamma\gamma$-fusion production of W pairs.

5. HEAVY CHARGED LEPTONS

We will now turn to the detection of a heavy charged lepton. This problem is useful, not only in its own right, but because it will lead us directly to the search for neutral Higgs bosons. It is also a process that is difficult to detect in a hadron collider.[9] For this exercise we have assumed a lepton mass of 250 GeV/c^2. After accounting for beamstrahlung and radiative effects, the effective R value is 2.3 at 1 TeV center-of-mass energy. The lepton, which we will label L, has only one

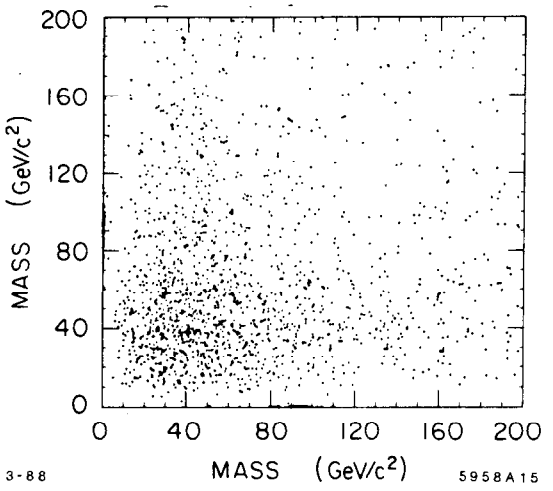

Fig. 9(a). Scatter plot of the jet mass in each hemisphere defined by the normal to the thrust axis for quark-pair production.

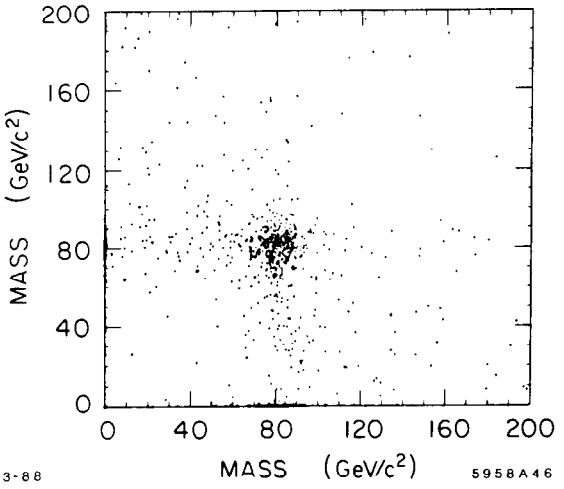

Fig. 9(b). Scatter plot of the jet mass in each hemisphere defined by the normal to the thrust axis for W-pair production.

decay mode:

$$L^- \rightarrow W^- \nu_L. \tag{17}$$

Thus, the production of a L^+L^- pair will yield the final state of two W's and

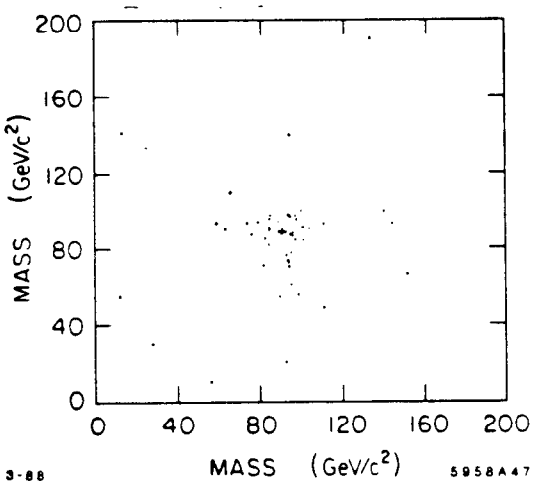

Fig. 9(c). Scatter plot of the jet mass in each hemisphere defined by the normal to the thrust axis for Z-pair production.

2ν's. One of the main backgrounds to L^+L^- production will thus be W^+W^- production, which differs only by the absence of the extra neutrinos.

As in the case of heavy quark production, there are two methods by which we could consider detecting the L^+L^- pair: the case in which both W's decay hadronicly or the case in which one W decays hadronicly and the other leptonicly. These cases are illustrated in Fig. 13.

With $E_{c.m.}$ and $p_{z_{c.m.}}$ unknown, case (d) in Fig. 13, W^+W^- pair production in which one W decays leptonicly, is a 0-C fit. Therefore, in general, case (b) in Fig. 13, L^+L^- pair production in which one L decays leptonicly will also fit it. This makes background suppression very difficult in the case in which there is a leptonic decay. Rick Van Kooten has analyzed this case and it turns out not to be completely hopeless. However the case in which both W's decay to hadrons is much superior and we will only consider that case here.

There are two additional backgrounds, illustrated in Fig. 14, which we have to consider. The first is WW-fusion production of W pairs [Fig. 14(a)]. This process, which has been calculated by Gunion and Tofighi-Niaki,[10] is an irreducible background because it leads to the identical final state as L^+L^- production.

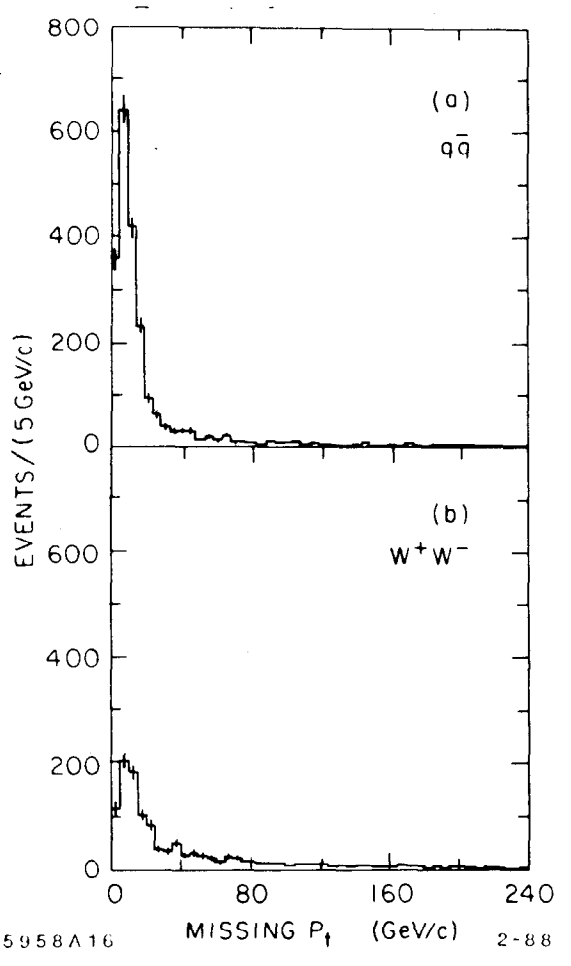

Fig. 10(a-b). The event transverse momentum for (a) quark-pair production and (b) W-pair production.

Fortunately its cross section is small, about 6% of the L^+L^- production cross section, and it peaks at lower WW invariant mass.

The second background [Fig. 14(b)] is the production of a WZ pair from γW fusion. This background was discussed at the La Thuile workshop.[8]) This is an insidious background for the following reasons:

1. Since one lepton couples to a γ, it develops no appreciable transverse momentum and escapes undetected down the beam pipe.
2. Since the other lepton couples to a W, the resulting neutrino carries away

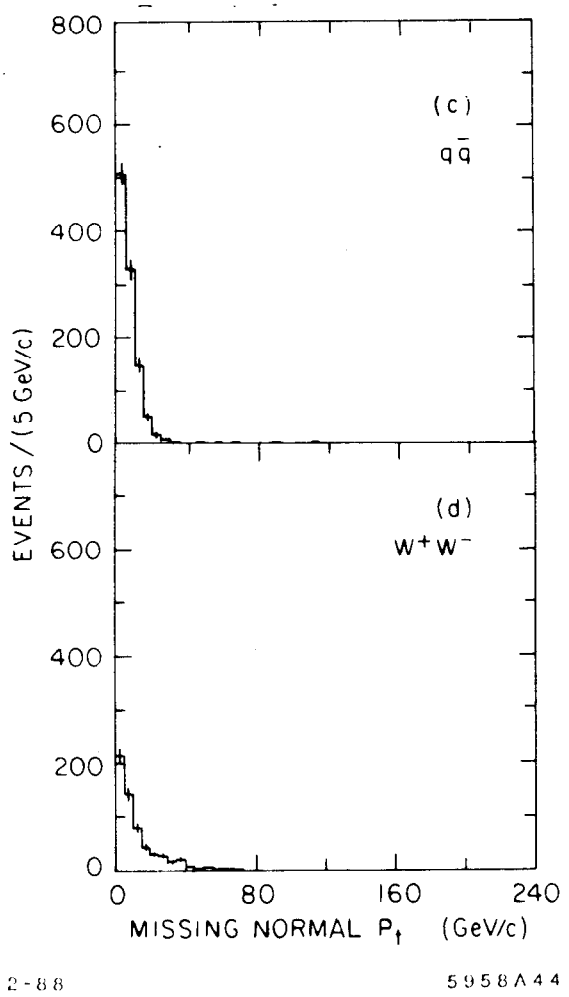

Fig. 10(c-d). The event transverse momentum normal to both the incident beams and the thrust axis for (c) quark-pair production and (d) W-pair production.

transverse momentum of order the W mass.

3. The cross section is large, of order the point cross section, perhaps half of the L-pair production cross section.

In other words, the $\gamma\gamma$-fusion and WW-fusion processes are relatively benign, the former because it does not develop missing transverse momentum and the latter because the cross section is small. The γW-fusion process has the worst features of both — it is relatively large and it does develop missing transverse

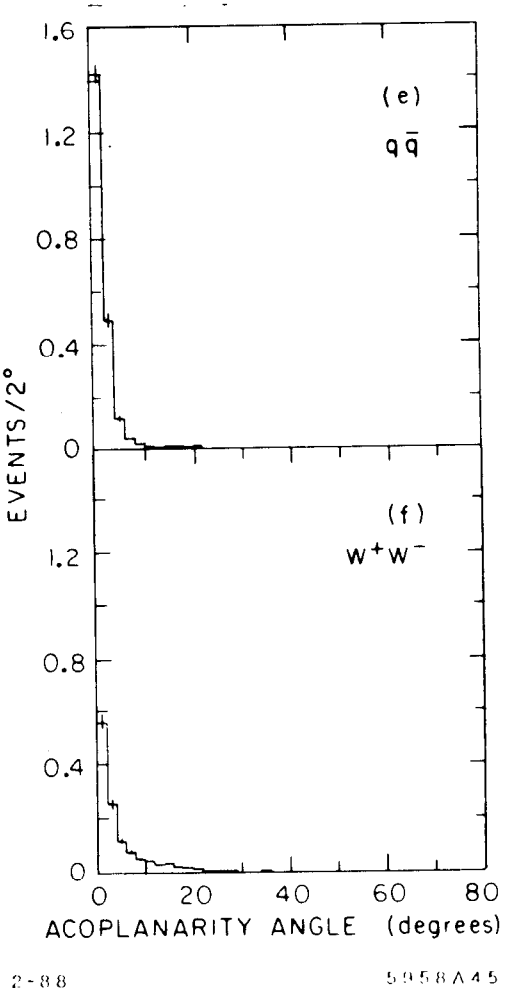

Fig. 10(e-f). The acoplanarity angle for (e) quark-pair production and (f) W-pair production.

momentum. This background also suggests another class of backgrounds that need investigation: $e^+e^- \rightarrow e^{\pm}\nu q\bar{q}'$.

There are, however, three mitigating factors to consider concerning the γW-fusion production of WZ background:

1. The mass of the W is not equal to the mass of the Z. Our normal mass cuts will reduce the background by a factor of two.

2. The WZ system has an odd rather than even number of charged tracks.

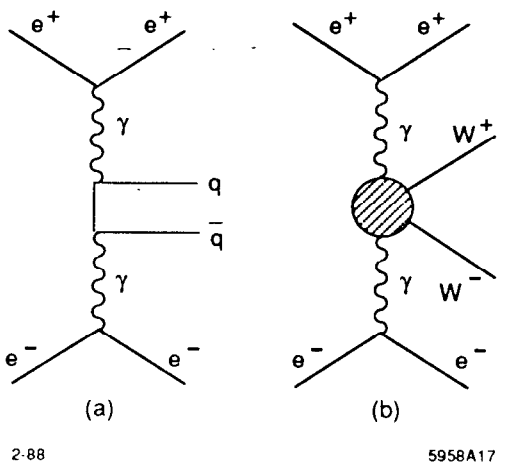

Fig. 11. Diagrams for (a) $q\bar{q}$ and (b) W^+W^- production by $\gamma\gamma$ fusion. The scattered e^+ and e^- in general go forward and are not detected. The shaded area in (b) represents the sum of all gauge-invariant couplings.

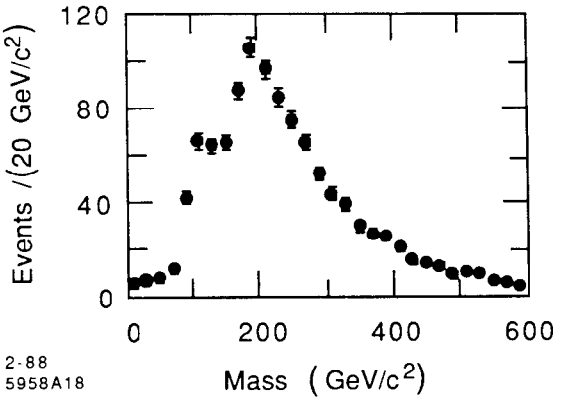

Fig. 12. The invariant mass spectrum of W pairs from $\gamma\gamma$-fusion production of W pairs. The figure represents 2 fb^{-1} of data at 1 TeV center-of-mass energy.

3. The process is completely calculable (and measurable with lower statistics) and can be subtracted with high precision.

Table 4: Cross Sections for W^+W^- Production from the Annihilation and the $\gamma\gamma$ Processes Including the Effects of Beamstrahlung

Process	R	R ($m_{vis} > 0.3$)
$e^+e^- \rightarrow W^+W^-$	41	28
$e^+e^- \rightarrow W^+W^-e^+e^-$	7	1.8

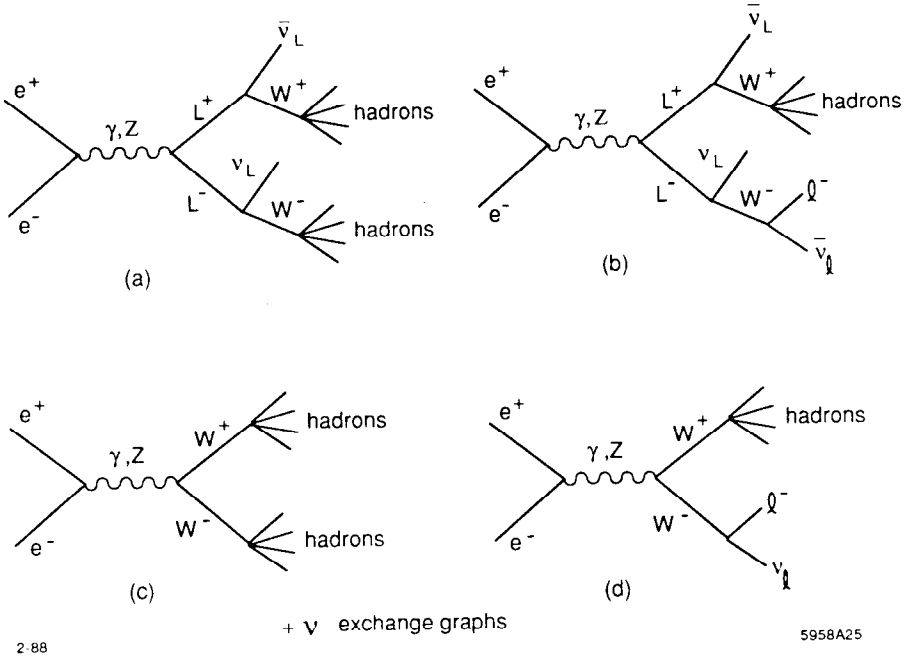

Fig. 13. Diagrams for an L^+L^- pair (a) in which both W's decay hadronicly and (b) in which one W decays hadronicly and the other decays leptonicly, and (c) and (d) for similar cases for W^+W^- pair production.

We will not consider the γW-fusion background further here, but it is clear that it will have to be included in future, more detailed studies.

The analysis of L^+L^- detection is relatively straight-forward:

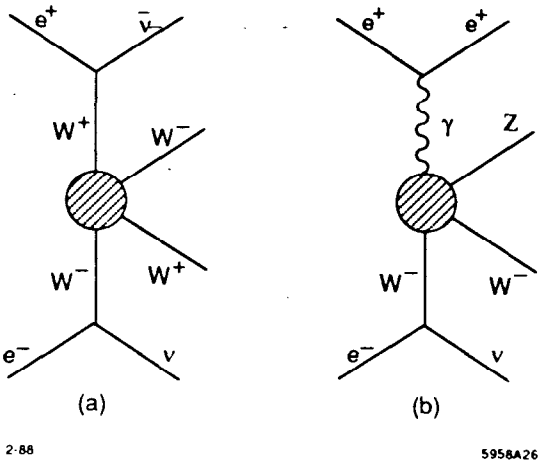

Fig. 14. (a) WW fusion and (b) γW fusion diagrams. The scattered e^+ in (b) in general goes forward and is not detected. The shaded areas represent the sum of all gauge-invariant couplings.

1. Lorentz transform the event along the direction of the incident beams (z-axis) so that $\sum \vec{p}_z = 0$, where the sum is over the visible charged and neutral particles.
2. Divide the event into two hemispheres using the thrust axis and require that $|\cos\theta_{thrust}| < 0.8$.
3. Require that the invariant mass in each hemisphere is within 10 GeV/c^2 of the W mass.
4. Require that the acoplanarity angle between the sum of the momenta in each hemisphere to be greater than 10°.

The results of this analysis are shown in Table 5. The largest background comes from irreducible WW fusion process. The other backgrounds are negligible. The invariant mass spectrum of the W pairs is shown in Fig. 15 along with that from WW fusion.

Table 5: Results for Heavy Lepton Analysis

	Events	Overall Efficiency	Signal/ Background
Backgrounds			
$q\bar{q}$	2	2×10^{-5}	
W^+W^-	13	13×10^{-5}	
ZZ	1	16×10^{-5}	
ZZ	41	0.11	
Total Background	57		
Signal			
L^+L^-	680	0.11	11.9

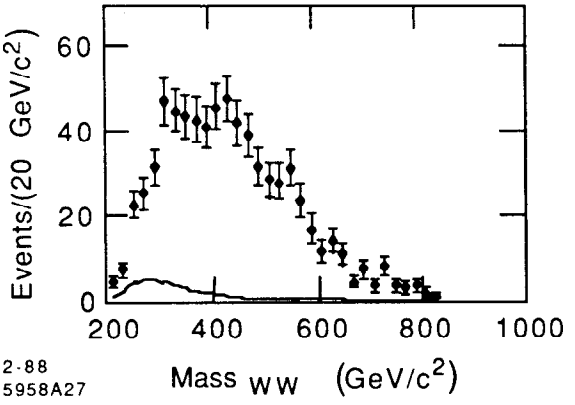

Fig. 15. The invariant mass spectrum of detected W^+W^- pairs from L^+L^- production (data points). The solid curve represents the spectrum from W^+W^- production by WW fusion.

6. STANDARD HIGGS

6.1. Introduction

The outstanding missing piece of the standard model is the origin of the spontaneous breaking of gauge symmetry. The search for this missing piece should

be the primary concern of all high-energy colliders.

The simplest way the standard model can be made consistent is by the addition of a single neutral Higgs boson. There are two major ways of producing this minimal Higgs boson in e^+e^- collisions, by annihilation into ZH and by WW fusion. Diagrams for these processes are shown in Fig. 16.

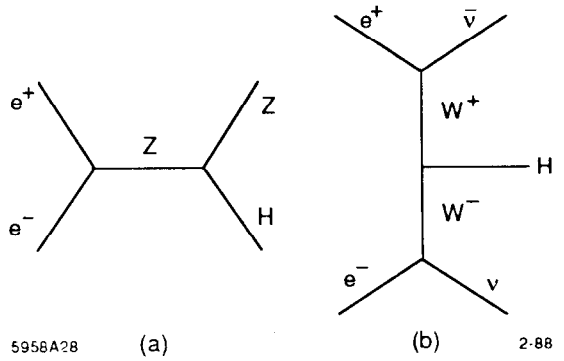

Fig. 16. Diagrams for Higgs boson production in e^+e^- collisions: (a) ZH production by annihilation and (b) H production by WW fusion.

The ZH mode will be used on the Z at the SLC and LEP (with the first Z real and the second Z virtual) and at LEP II (with the first Z virtual and the second Z real). Pat Burchat has analyzed this mode for the TLC. It can be used as a verification, but the WW-fusion process is always superior at high energy. The cross section dependence, taken from a paper by Altarelli, Mele, and Pitolli[11] is shown in Fig. 17. At 1 TeV, the cross section for the WW-fusion process is 20 times larger than the annihilation process.

Higgs detection via WW fusion can be divided into two cases:

1. $m_H \gg 2m_W$. In this case $H \rightarrow W^+W^-$or ZZ, with the bosons well separated.
2. $m_H \lesssim 2m_W$. In this case $H \rightarrow W^+W^-$ with the W's not well separated or $H \rightarrow t\bar{t}$ or $b\bar{b}$, depending on what is kinematically allowed.

We will consider these two cases separately.

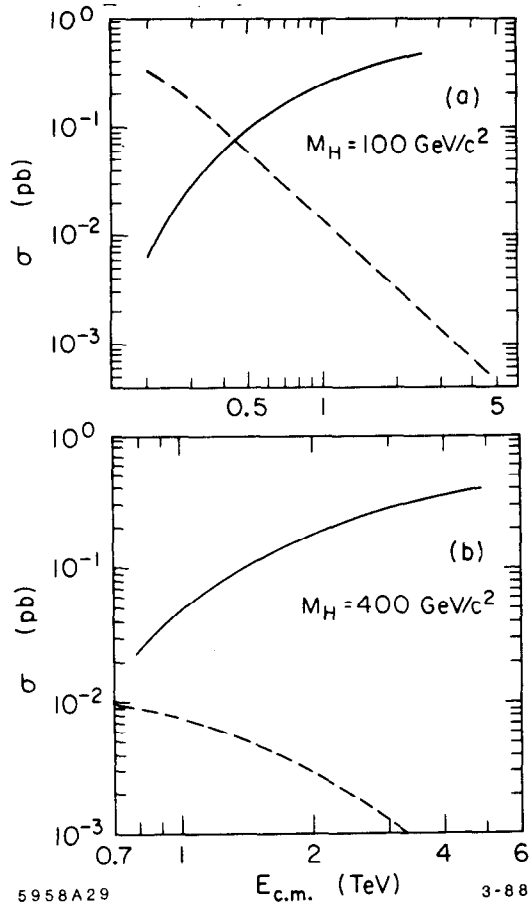

Fig. 17. Cross sections for (a) 100 GeV/c^2 and (b) 400 GeV/c^2 Higgs boson production in e^+e^- collisions. The solid curve represents the WW-fusion process, $e^+e^- \rightarrow W^+W^-\nu\bar{\nu}$, and the dashed curve represents the annihilation process, $e^+e^- \rightarrow ZH$.

6.2. High-Mass Higgs Boson

The final state is either $W^+W^-\nu\bar{\nu}$ or $ZZ\nu\bar{\nu}$. Note that this is the analysis we have just done for the case of L^+L^- production. The only thing we have to change is to expand the mass cut to have the hemisphere masses be either within 10 GeV/c^2 of the W mass or the Z mass. Looking forward to this analysis, I took the liberty of making this expansion already in Fig. 15. (It made no difference because there was essentially no background.)

To make this problem a little more challenging, we will show the results for various mass Higgs bosons on top of a background from a heavy lepton. Fig. 18 shows the results for 300, 400, and 500 GeV/c^2 Higgs bosons. In the 300 and 400 GeV/c^2 cases, the Higgs stands out easily over the heavy lepton background. It gets lost in this background when its mass reaches 500 GeV/c^2, but stands out well if there is no heavy lepton background [Fig. 18(d)]. The $W^+W^-\nu\bar{\nu}$ production shown by the solid line in Fig. 18 can be thought of as the non-resonant WW scattering, or alternatively, as the mass spectrum of a Higgs boson with infinite mass.

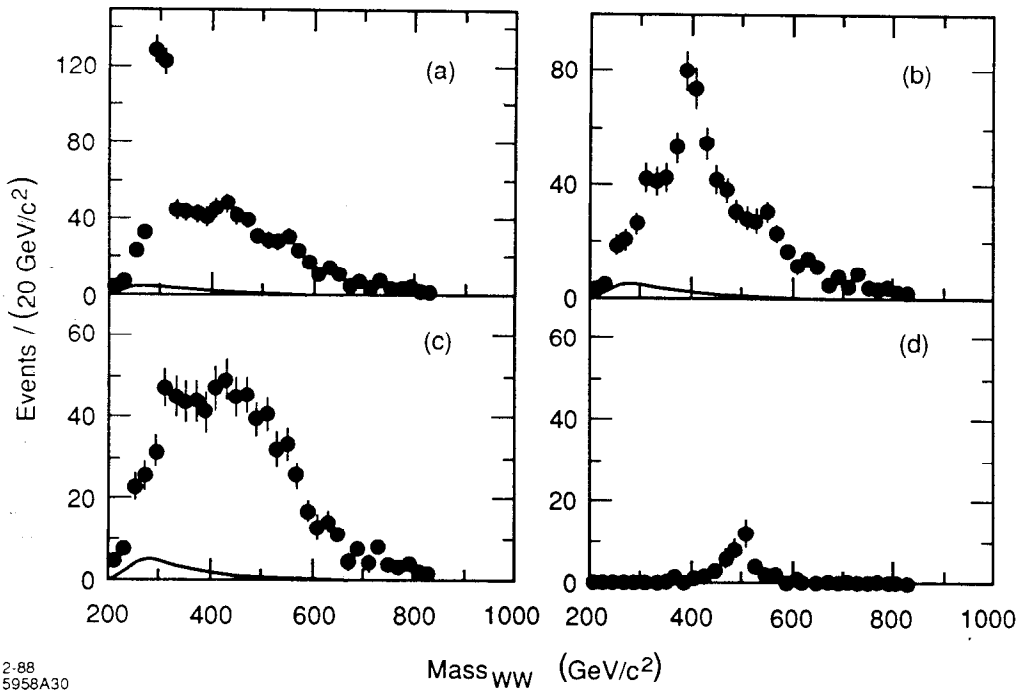

Fig. 18. The invariant mass of detected W^+W^- pairs from the sum of a 250 GeV/c^2 heavy lepton and a (a) 300 GeV/c^2, (b) 400 GeV/c^2, or (c) 500 GeV/c^2 neutral Higgs boson. (d) shows just the contribution of the 500 GeV/c^2 Higgs. The solid line represents the non-resonant W^+W^- production by WW fusion.

The upper limit of detectability of a minimal Higgs with our assumed 30 fb^{-1}

of data is probably about 500 or 600 GeV/c^2. Figure 19 shows the number of detected events and the width of the Higgs. The width increases as the cube of the mass, making the detection of masses above 600 GeV/c^2 rather difficult.

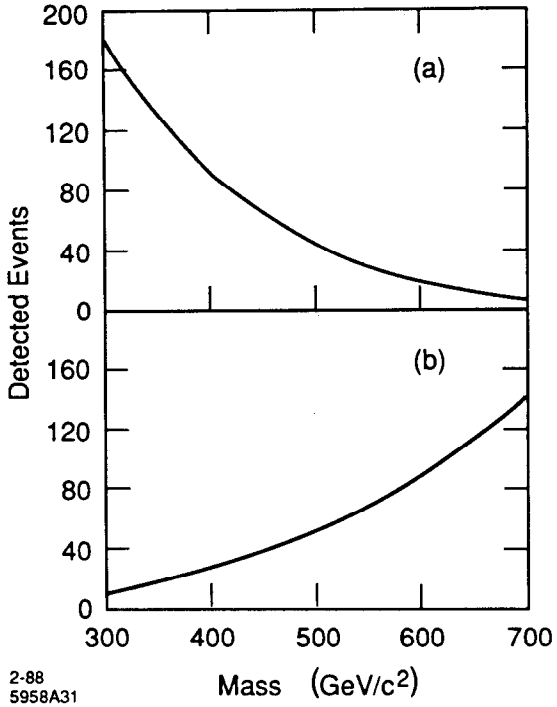

Fig. 19. (a) Number of detected Higgs bosons in 30 fb^{-1} at 1 TeV center-of-mass energy as a function of the mass of the Higgs. (b) The width of the minimal Higgs boson as a function of its mass.

6.3. Intermediate-Mass Higgs Boson

This case is particularly interesting because it is a rather difficult, and in some cases impossible, problem in hadron colliders. We will see that it causes no difficulty in a e^+e^- collider.

The analysis can proceed in much the same way as in the high-mass case, except that the requirement that $m_{jet} = m_W$ can no longer be made. There are also some additional backgrounds that must be considered in some mass ranges.

The process of Z production by WW-fusion, $e^+e^- \rightarrow Z\nu\bar{\nu}$, which is shown in Fig. 20, has been calculated by Mike Peskin. The cross section for this process is three times larger than that for Higgs production at the same mass. Thus for $m_H \approx m_Z$, the best way to find the Higgs is to measure that these "Z's" have $b\bar{b}$ branching fractions twice normal or $t\bar{t}$ branching fractions several times normal.

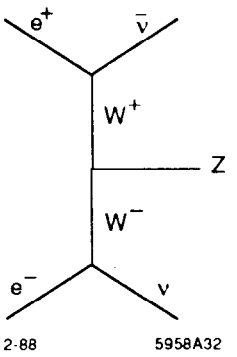

Fig. 20. Diagram for Z production by WW fusion.

There are also additional insidious γW-fusion processes, as shown in Fig. 21. The single W production diagram has an enormous cross section, 136 units of R.[12] As we have mentioned previously, these backgrounds can be suppressed experimentally by noting that an odd number of charged particles have been detected.

The analysis for intermediate-mass Higgs bosons was done by Dave Burke. It has the same spirit of the analyses we have looked at so far, but varies in some details. The steps of the analysis are

1. Force the cluster finder to find two jets.
2. For both jets require that $|\cos\theta_j| < 0.7$, where θ_j is the angle between the beam direction and the jet axis.
3. Require that the missing transverse momentum in the event lie between 50 and 150 GeV/c.

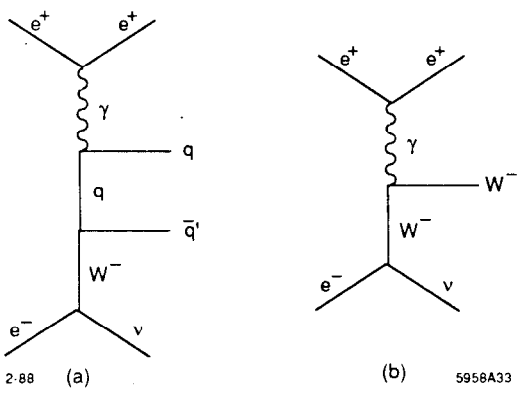

Fig. 21. Diagrams for (a) $q\bar{q}'$ and (b) single W production by γW fusion.

4. Require that there be no isolated leptons in the event.

5. Require each jet to satisfy a mass constraint appropriate to the Higgs mass being searched for.

Figure 22 shows the results for 200 and 150 GeV/c^2 Higgs bosons. In the former case the Higgs decays primarily to W pairs, but the decay products of the W's do not separate spatially because the W have little momentum. In this case the appropriate mass constraint is that $m_{jet} > 20$ GeV/c^2. In the latter case, the Higgs is assumed to decay into a $t\bar{t}$ pair with the top quark mass set at 50 GeV/c^2. In this case, the appropriate mass constraint is that m_{jet} lie between 30 and 70 GeV/c^2. In both cases, there is little background from other sources.

Figure 23 shows the cases of 50 and 120 GeV/c^2 Higgs bosons. In these cases the Higgs bosons are assumed to decay into $b\bar{b}$ pairs. The appropriate mass constraint here is that $m_{jet} < 40$ GeV/c^2. The third peak in Fig. 23 is from WW-fusion production of a single Z.

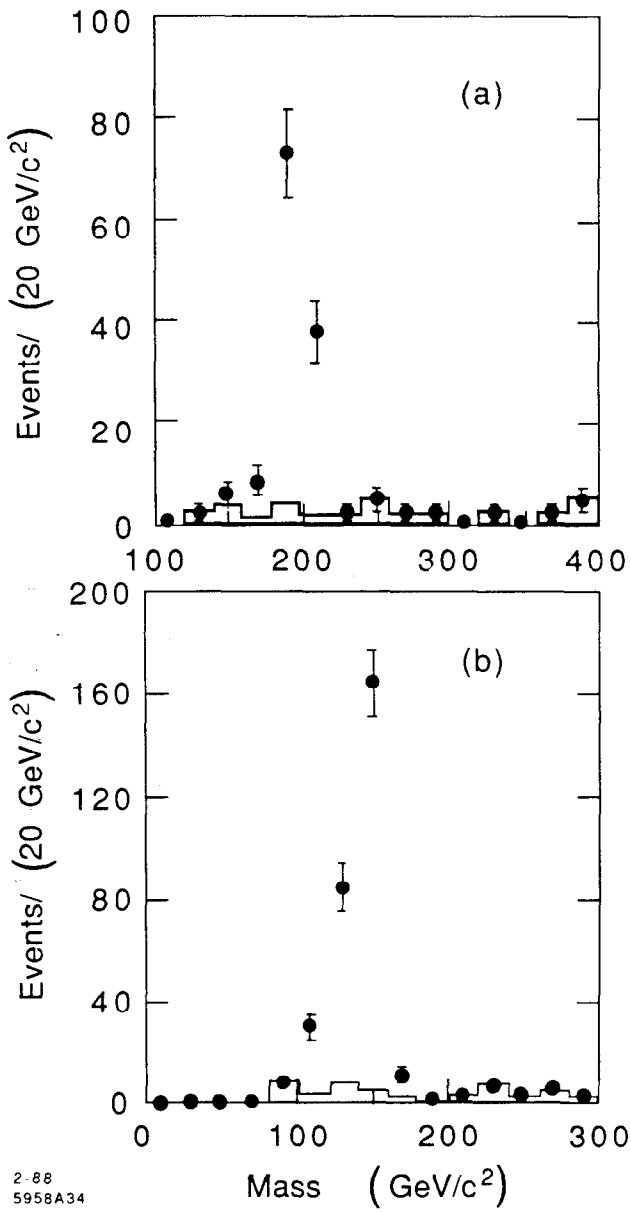

Fig. 22. The invariant mass of detected particles for the case of a (a) 200 GeV/c^2 Higgs boson that decays into vector bosons and a (b) 150 GeV/c^2 Higgs boson that decays into 50 GeV/c^2 top quark pairs. The histogram represents backgrounds from all sources except γW-fusion. In (a) each jet was required to have a mass greater than 20 GeV/c^2 and in (b) each jet was required to have a mass between 30 and 70 GeV/c^2.

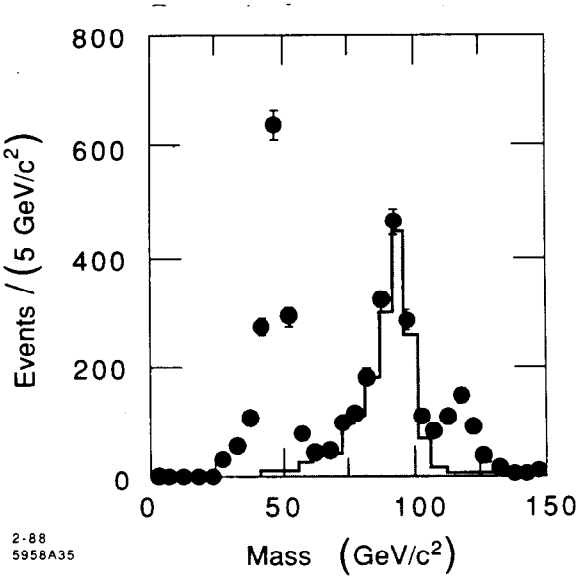

Fig. 23. The invariant mass of detected particles for the cases of 50 and 120 GeV/c^2 Higgs bosons, which are assumed to decay into $b\bar{b}$ pairs. Each jet was required to have a mass less than 40 GeV/c^2. The histogram represents backgrounds from all sources except γW-fusion. The peak at the Z mass is due to WW-fusion production of a single Z. between 30 and 70 GeV/c^2.

7. CHARGED HIGGS BOSONS

Charged Higgs bosons will be produced in any extension of the minimal Higgs sector. They, or something very much like them, are required in any model that tries to avoid the unnaturalness of the minimal standard model.

Charged Higgs bosons are pair produced with a cross section

$$\sigma \approx \frac{1}{3}\beta^3 \sigma_{pt}. \tag{18}$$

They have the curious property of not coupling to vector bosons at the tree level — an H^+W^-Z coupling does not occur in the standard lagrangian. Thus, the normal decay of a high-mass Higgs is to the highest mass quarks: $H^+ \rightarrow t\bar{b}$. It is this property that makes the charged Higgs undetectable at hadron colliders.[13)]

The analysis, which is the most complicated one that we have had to discuss, was done by Sachio Komamiya. The steps are as follows:

1. Require that the visible energy is greater than 70% of the center of mass energy.
2. Force the cluster finder to find four jets.
3. Choose which of the three combinations of jet pairings to use by minimizing a χ^2:

$$\chi^2 = \left(\frac{\frac{1}{2}E_{c.m.} - E_i - E_j}{\frac{1}{2}E_{c.m.}}\right)^2 + \frac{1}{4}\left[\left(\frac{m_{ij} - m_H}{m_H}\right)^2 + \left(\frac{m_{kl} - m_H}{m_H}\right)^2\right], \quad (19)$$

   where E_i are the jet energies that have been rescaled so that their sum equals $E_{c.m.}$, and m_H is a scanned parameter.

4. Require the following quality cuts:
   (a) $E_i > 30$ GeV for all i,
   (b) $|m_{H+} - m_{H-}| < 40$ GeV/c^2,
   (c) $|E_{H+} - E_{H-}| < 20$ GeV, and
   (d) $\psi_{ij} > 50°$, where ψ_{ij} is the angle between any two jets. This last requirement is tuned slightly for different Higgs mass ranges.
5. Require that there be at least three particles with $p > 1$ GeV/c and $0.2 < \delta < 2$ mm, where δ is the transverse distance of closest approach to the interaction point.

There are a couple of things to note about this analysis:

1. Unlike all of the other analyses, there is an attempt here to use all four energy-momentum constraints by requiring that the visible energy be approximately equal to the center-of-mass energy. Note however, that this is only used to choose the correct pairing of jets.
2. The final requirement reduces the background substantially. The reason is that there are four (long-lived) b quark decays in each signal event and normally at most two b quark decays in each background event.

Fig. 24 shows the resulting signals and backgrounds for 120, 200, and 300 GeV/c^2 charged Higgs bosons. In all cases, the signal easily dominates the background.

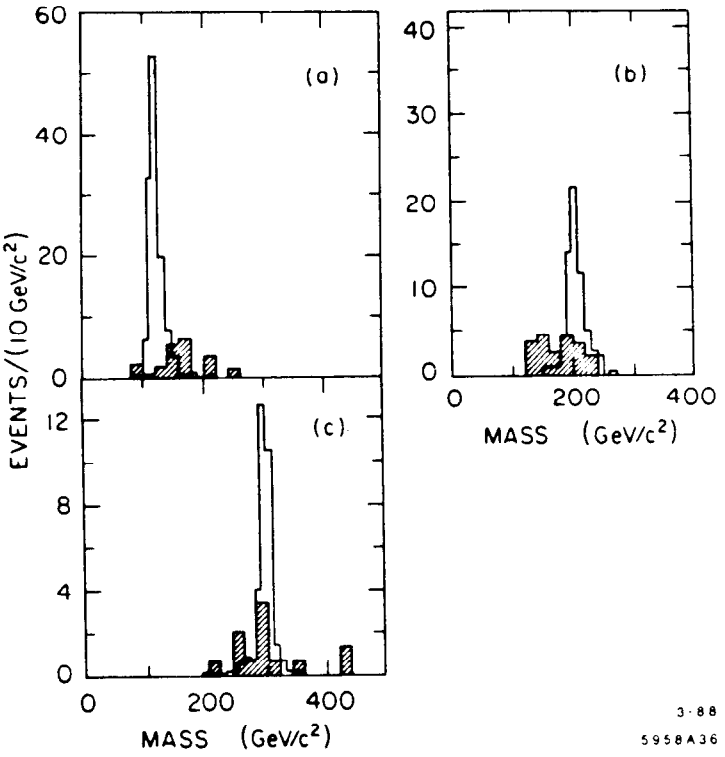

Fig. 24. Signal and background (shaded) for (a) 120, (b) 200, and (c) 300 GeV/c^2 charged Higgs bosons. Case (a) was run for 10 fb^{-1} of luminosity at $E_{c.m.} = 600$ GeV, which scales to 23 fb^{-1} of luminosity at $E_{c.m.} = 1$ TeV; case (b) was run for 10 fb^{-1} of luminosity at $E_{c.m.} = 600$ GeV, which scales to 15 fb^{-1} of luminosity at $E_{c.m.} = 1$ TeV; and case (c) was run for 10 fb^{-1} of luminosity at $E_{c.m.} = 1$ TeV.

Figure 25 shows the rate of detected charged Higgs pairs for our standard run of 30 fb^{-1} of luminosity at 1 TeV. The limit of sensitivity is at a mass of about 400 GeV/c^2.

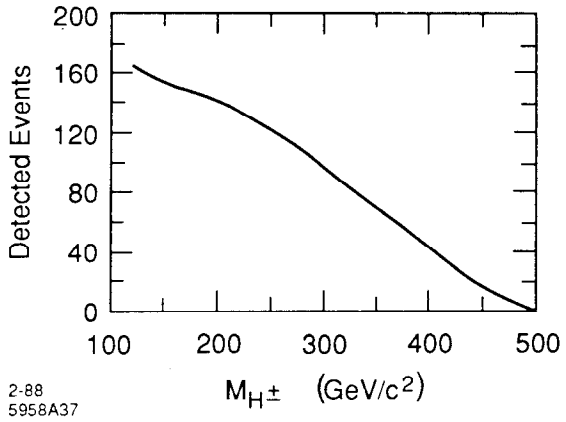

Fig. 25. Number of detected charged Higgs boson pairs in 30 fb^{-1} at 1 TeV center-of-mass energy as a function of the mass of the Higgs.

8. PROSPECTS

We have seen that the physics of e^+e^- linear colliders is extremely attractive. These colliders will fill crucial holes in the physics capabilities of hadron colliders, and they will allow a more detailed study of the effects that may be seen in hadron colliders.

The technical design work is at a very early stage. We should see a great deal of progress and a convergence of views as research and development progresses over the next few years.

Linear colliders clearly have an important role in the future of particle physics; we should vigorously pursue planning, research, and development on them.

REFERENCES

1. Material in this talk is drawn heavily from lectures that Mike Peskin and I gave at the 1987 SLAC Summer Institute on Particle Physics (G. J. Feldman, SLAC report number SLAC-PUB-4563 and to be published).

2. B. Richter, *Nucl. Instrum. Methods* **136**, 47 (1976).

3. Advisory Panel on the Prospects for e^+e^- Linear Colliders in the TeV Range, CERN report number CLIC note 38 (May, 1987) and K. Johnsen in the *Proceedings of the Workshop on Physics at Future Accelerators,* La Thuile, Italy and Geneva, Switzerland, January 1987, CERN report number CERN-87-07 (1987). There are some detailed differences between these two reports. I have tried to take a consistent set of parameters.

4. R. J. Noble, *Nucl. Instrum. Methods* **A256**, 427 (1987); R. Palmer, SLAC report number AAS Note 30 (1987). See also P. Chen, SLAC report number SLAC-PUB-4379 (1987).

5. See, for example, C. Dib and F. J. Gilman, *Phys. Rev. D* **36**, 1337 (1987).

6. G. J. Feldman, SLAC report number SLAC-PUB-4563 (1988).

7. R. Wigmans, NIKHEF report number NIKHEF-H/87-12 (1987).

8. D. Froidevaux in the *Proceedings of the Workshop on Physics at Future Accelerators,* La Thuile, Italy and Geneva, Switzerland, January 1987, CERN report number CERN-87-07 (1987).

9. V. Barger, T. Han, and J. Ohnemus, University of Wisconsin report number MAD/PH/331 (1987), but see also Ref. 8.

10. J. F. Gunion and A. Tofighi-Niaki, *Phys. Rev. D* **36**, 2671 (1987).

11. G. Altarelli, B. Mele, and F. Pitolli, *Nucl. Phys.* **B287**, 205 (1987).

12. E. Gabrielli in the *Proceedings of the Workshop on Physics at Future Accelerators,* La Thuile, Italy and Geneva, Switzerland, January 1987, CERN report number CERN-87-07 (1987).

13. H.-U. Bengtsson, H. Yamamoto, and S. Komamiya, SLAC report number SLAC-PUB-4369 (1987).